Journal Pre-proofs

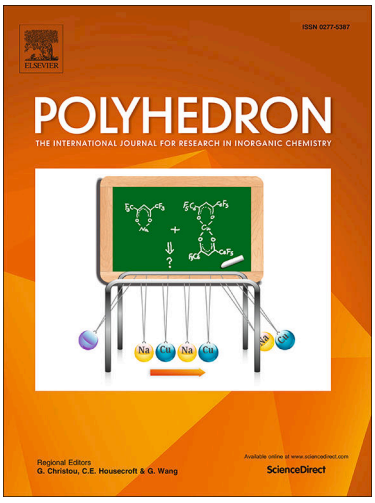

(η ^{6}-Arene) ruthenium(II) complexes with ferrocene-tethered salicylaldimine ligands: synthesis, characterization and anti-cancer properties

Jakku Ranjith Kumar, Eda Rami Reddy, Nedaossadat Mirzadeh, T. Srinivasa Reddy, Anil Kumar Vardhaman, L. Giribabu, Balasubramanian Sridhar, Deep Pooja, Sistla Ramakrisna, Suresh Bhargava, Rajiv Trivedi

PII: S0277-5387(20)30486-1
DOI: https://doi.org/10.1016/j.poly.2020.114829
Reference: POLY 114829

To appear in: *Polyhedron*

Received Date: 22 July 2020
Revised Date: 30 September 2020
Accepted Date: 2 October 2020

Please cite this article as: J.R. Kumar, E.R. Reddy, N. Mirzadeh, T. Srinivasa Reddy, A. Kumar Vardhaman, L. Giribabu, B. Sridhar, D. Pooja, S. Ramakrisna, S. Bhargava, R. Trivedi, (η ^{6}-Arene) ruthenium(II) complexes with ferrocene-tethered salicylaldimine ligands: synthesis, characterization and anti-cancer properties, *Polyhedron* (2020), doi: https://doi.org/10.1016/j.poly.2020.114829

This is a PDF file of an article that has undergone enhancements after acceptance, such as the addition of a cover page and metadata, and formatting for readability, but it is not yet the definitive version of record. This version will undergo additional copyediting, typesetting and review before it is published in its final form, but we are providing this version to give early visibility of the article. Please note that, during the production process, errors may be discovered which could affect the content, and all legal disclaimers that apply to the journal pertain.

© 2020 Published by Elsevier Ltd.

Journal Pre-proofs

(η^6-Arene) ruthenium(II) complexes with ferrocene-tethered salicylaldimine ligands: synthesis, characterization and anti-cancer properties.

Jakku Ranjith Kumar,[a,b,c] Eda Rami Reddy,[a] Nedaossadat Mirzadeh,[*b,c] T. Srinivasa Reddy,[c] Anil Kumar Vardhaman,[d] L. Giribabu,[d] Balasubramanian Sridhar,[e] Deep Pooja,[f] Sistla Ramakrisna,[f] Suresh Bhargava,[*b,c] Rajiv Trivedi[*a,b]

[a] *Catalysis and Fine Chemicals Division, CSIR-Indian Institute of Chemical Technology, Uppal Road, Tarnaka, Hyderabad-500007, India.*

[b] *IICT-RMIT Centre, CSIR-Indian Institute of Chemical Technology, Uppal Road, Tarnaka, Hyderabad-500007, India.*

[c] *Centre for Advanced Materials and Industrial Chemistry (CAMIC), School of Science, RMIT University, GPO Box 2476, Melbourne, 3001, Australia.*

[d] *Polymer and Functional Materials Division, CSIR-Indian Institute of Chemical Technology, Uppal Road, Tarnaka, Hyderabad-500007, India.*

[e] *Analytical Division, CSIR-Indian Institute of Chemical Technology, Hyderabad 500007, India.*

[f] *Applied Biology Division, CSIR-Indian Institute of Chemical Technology, Hyderabad 500007, India.*

Correspondence to: suresh.bhargava@rmit.edu.au, nedaossadat.mirzadeh@rmit.edu.au, trivedi@iict.res.in, trivedi.iict@gov.in

Abstract: A series of ruthenium(II) complexes (**5a**-**5f**) derived from ferrocenyl salicylaldimine ligands (**3a**-**3f**), coordinated in a chelating mode through the deprotonated phenolic oxygen atom and the imine nitrogen, were synthesized and fully characterised. The molecular structures of selected ligands and complexes were also confirmed by X-ray diffraction analysis. The heterobimetallic Ru-Fe complexes **5a**-**5f** were evaluated for their *in vitro* anti-cancer activity against human liver cancer (HepG2) and human cervical cancer (HeLa) cell lines and showed better activities compared to the ferrocenyl salicylaldimine ligands. Among the heterobimetallic complexes, **5c** and **5d** showed enhanced cytotoxicity against HeLa cancer cells (IC_{50} value of 9.34 µM compared to 31.32 µM for cisplatin), and HepG2 cancer cells (IC_{50} value of 15.74 µM compared to 27.95 µM for cisplatin), respectively. Mechanistic studies indicated compound **5d** induced cell cycle arrest in the S phase. Further, compound 5d treatment resulted in increased ROS generation and loss of mitochondrial membrane potential in HepG2 cells.

Keywords: Ferrocene, salicylaldimine ligands, Ruthenium complexes, Anti-cancer activity

1.0 Introduction

The anti-cancer properties of metal containing drugs is an extensively researched area. Notably, the antiproliferative activity of the square planar platinum(II) complex *cis*-diamminedichloroplatinum(II), [*cis*-$Pt(NH_3)_2Cl_2$], discovered by Barnett Rosenberg in the 1960s[1,2] has led to the treatment of several types of cancers, including testicular, head and neck.[3] However, the range of side effects, including oto-, neuro- and nephrotoxicities, are severe limitations to its clinical use. In view of this aspect, other transition metal-based drugs have been investigated as alternatives to platinum-based therapies and in recent years, ruthenium-based drugs have shown great potential in chemotherapy. For instance, $(H_2im)[RuCl_4(DMSO)(Him)]$ (NAMI-A, Him = 1*H*-imidazole) and, $Na[RuCl_4(Hind)_2]$ (NKP-1339, Hind = 1*H*-indazole) are among the most prominent ruthenium complexes that have entered various stages of clinical trials.[4] Furthermore, the half-sandwich arene ruthenium complexes, RAPTA[5] and RAED[6] compounds, have been the most extensively investigated organoruthenium complexes (Figure 1**)**. According to Sadler and co-workers, the electronic properties of the Ru(II) complexes are significantly affected by the change of donor ligand.[7] This change in ligand had direct consequence on the nucleobase to be targeted. Subsequent studies were performed to establish the structure-activity relationships of Ru(II) complexes with various chelating *N*,*N*-(diamines and bipyridine), *N*,*O*-(amino acids) and *O*,*O*-(acetylacetonate) ligands.[8] It has been shown that the presence of two non-leaving *cis*-coordinated amine ligands was crucial for the anti-cancer properties of platinum complexes.[9] Numerous metal complexes, including ruthenium compounds, containing aromatic *N*-donor ligands (phenanthroline, pyridine, and imidazole) have exhibited promising anti-cancer properties.[10] Free N-H moieties in the ligand of Ru(II) complexes often facilitates an effective and strong interaction with DNA via hydrogen bonding interactions.[11]

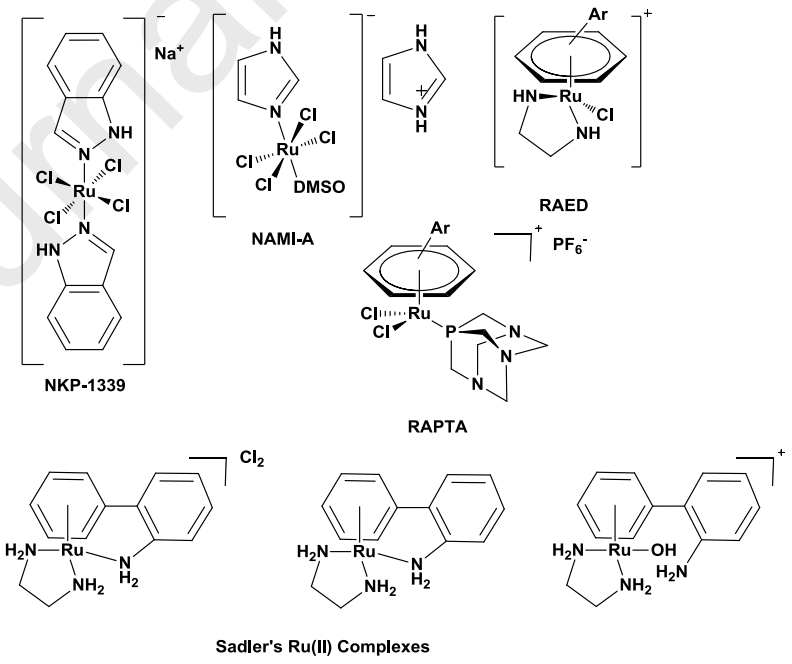

Figure 1. Examples of ruthenium-based bioactive complexes.

Journal Pre-proofs

By introducing a second metal into potential anti-cancer agents, a new variant of the metallodrugs can be examined.[12] One of the most abundant metals, iron, as its organometallic complex ferrocene, has gained much attention in the field of medicinal chemistry.[13] Heterobimetallic complexes containing a ferrocenyl ligand exhibit different electrochemical and biological properties compared to those observed for the free ligand. Furthermore, there are examples of ferrocenyl motifs incorporated into heterobimetallic assemblies in which the ferrocene fragment, a chemically robust moiety having low toxicity, acts as a one-electron reservoir.[14] The ferrocene moiety is stable in both aqueous and aerobic media, and its favorable electrochemical properties make it a prominent molecule for use in biological applications.[13] The chemotherapeutic application of the ferrocene moiety is associated with its electrochemical activation wherein the oxidation of iron atom produces the ferrocenium (Fc^+) species, which can assist in producing reactive oxygen species (ROS).[15] Similar redox processes are known to play pivotal roles in many metal-containing therapeutics.[16] In an attempt to design and develop heterobimetallic cytotoxic anti-cancer agents, different metal complexes containing gold, silver, palladium, rhodium and iridium[17] have been coordinated with ferrocenyl-containing ligands to achieve a synergistic effect between the two active metals. In addition, examples where ruthenium and iron have been combined within the same molecule and their anti-cancer activity investigated have been reported (Figure 2).[14]

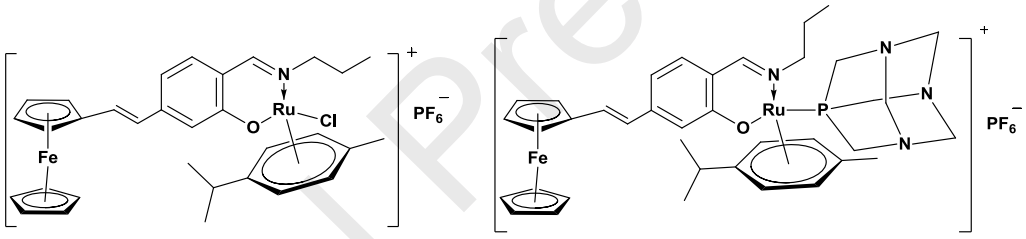

Figure 2. Structures of ferrocenyl-ruthenium anti-cancer complexes.

Recent work by Štěpnička and co-workers have shown that di- and tri-nuclear heterobimetallic complexes containing ferrocenyl and arene-ruthenium fragments exhibited moderate cytotoxic activities against cisplatin-sensitive (A2780) and cisplatin-resistant (A2780cisR) human ovarian cancer cell lines,[18] and Ramadevi and co-workers have investigated ruthenium-arene complexes containing *N*-ferrocenyl amino acids against MCF7 cell line.[19] There are also a number of reports on ferrocene-free Schiff base complexes containing the (*p*-cymene)Ru(II) moiety that exhibit a range of *in vitro* antiproliferative activities against cell lines such as, human metastatic breast carcinoma MDA-MB-231, human pancreatic carcinoma MIA PaCa-2, hepatocellular carcinoma Hep G2 and human lung cancer A549.[20] As an extension of this fascinating chemistry to deliver novel Ru-based drugs, we have designed and prepared the (η^6-arene)ruthenium(II) half-sandwich complexes **5a**-**5f**. Synthesized from the reaction of ferrocenyl salicylaldimine ligands with [Ru(*p*-cymene)Cl_2]$_2$, these heterobimetallic complexes adopt "piano-stool" geometry which offers structural stability and the opportunity for tuning the electronic properties at the ruthenium center. Herein, we report the synthesis and characterization of a series of novel Ru(II) complexes bearing bidentate *N,O*-donor Schiff-base ligands, and the

in vitro anti-cancer activity against two different human cancer cell lines [HepG2 (human liver) and HeLa (human cervical)].

2.0 Experimental

2.1 Materials and Methods

Ferrocene, 4-nitroaniline, toluene, dichloro(*p*-cymene)ruthenium(II) dimer, and substituted salicylaldehydes were purchased from Sigma Aldrich and used as supplied. HepG2 human liver carcinoma cells and HeLa human cervical cancer cells were purchased from the American Type Culture Collection (ATCC) (Manassas, VA, USA). Dulbecco's modified eagle medium (DMEM), trypsin–EDTA, antibiotic/anti-mycotic solution, 3-(4,5-dimethylthiazol-2-yl)-2,5-diphenyl tetrazolium bromide (MTT), dimethyl sulfoxide (DMSO) were purchased from Sigma-Aldrich (St. Louis, MO, USA). Foetal bovine serum was purchased from Gibco, USA. Cell culture plasticware was purchased from Tarson Ltd (Mumbai, India). ^{1}H and ^{13}C NMR spectra were recorded at room temperature on a Bruker Avance 400 or Varian Inova 500 spectrometer as $CDCl_3$ solutions. Chemical shifts (δ) for protons are reported in ppm downfield from TMS as an internal standard and the carbon chemical shifts are referenced to the ^{13}C signal of $CDCl_3$ at 77.0 ppm. Coupling constants (*J*) are expressed in Hz. MALDI-TOF mass spectra were recorded on a Shimadzu Biotech Axima spectrometer. For MALDI-TOF and ESI mass spectra, *m/z* values are expressed in atomic mass units. FT-IR spectra were recorded on a Thermo Nicolet Nexus 670 spectrometer as KBr discs. Melting points were determined using a Toshniwal apparatus and are uncorrected. The UV-vis. spectra were recorded on a UV 3600 Shimadzu spectrophotometer over the range of 200-550 nm as CH_3CN solution. Cyclic voltammetry (CV) experiments were performed using a conventional three-electrode configuration consisting of a glassy carbon working electrode, a platinum wire auxiliary electrode, and a saturated calomel (SCE) reference electrode. The cyclic voltammograms were recorded on a CHI620 model electrochemical analyzer in the presence of 0.1 M tetrabutylammonium perchlorate (TBAP) supporting electrolyte at a scan rate of 0.1 Vs^{-1}. Elemental analyses were performed with an Elementary Vario MICRO analyzer. All reactions were carried out in the absence of air using standard Schlenk techniques unless stated otherwise. Solvents were deoxygenated, purified and dried prior to use.

2.2 General procedure for the synthesis of ligands 3a-3f

4-Ferrocenyl aniline (**1**) was synthesized in two steps by a reported method.[23] Under a nitrogen atmosphere, a two-neck round bottom flask equipped with magnetic stirrer was charged with the appropriate salicylaldehyde **2a**-**2f** (1 mmol) followed by a solution of 4-ferrocenyl aniline 4-nitrophenyl ferrocene (277 mg, 1 mmol) in dry ethanol (10 mL). *p*-Toluene sulfonic acid (3-4 mg) was added then the reaction mixture to stir for 4 hours at room temperature and the precipitated solid was collected by suction filtration, washed with cold dichloromethane and dried under vacuum. The product was purified by recrystallization from dichloromethane/hexane.

Ligand 3a

Reaction of 4-ferrocenyl aniline (277 mg, 1 mmol) and 4-nitrosalicylaldehyde (**2a**) (167.12 mg, 1 mmol) gave **3a** as an orange red crystalline solid, yield: 80%. ^{1}H NMR (500 MHz, $CDCl_3$): δ (ppm)= 14.63 (s, 1H, -OH), 8.77 (s, 1H, CH=N), 8.40 (d, J = 2.7 Hz, 1H, ArH), 8.30 – 8.24 (m, 1H, ArH), 7.58 – 7.53 (m, 2H, ArH), 7.30 – 7.27 (m, 2H, ArH), 7.10 (d, J = 9.2 Hz, 1H, ArH), 4.71 (s, 2H, C_5H_4), 4.40 (s, 2H, C_5H_4), 4.11 (s, 5H, C_5H_5). ^{13}C NMR (101 MHz, $CDCl_3$): δ (ppm) = 161.59, 157.21, 147.54, 134.03, 128.08, 126.96, 121.65, 118.21, 115.61, 84.38, 69.73, 69.31, 66.58, 18.36. ESI: *m/z* 427 $[M+H]^+$

Ligand 3b

Reaction of 4-ferrocenyl aniline (277 mg, 1 mmol) and salicylaldehyde (2b) (122 mg, 1 mmol) gave (3b)as an orange red crystalline solid, yield: 82%.^{1}H NMR (400 MHz, $CDCl_3$): δ 13.32 (s, 1H, -OH), 8.62 (s, 1H, CH=N), 7.47 – 7.44 (m, 2H, ArH), 7.32 (dd, *J* = 15.4, 8.1 Hz, 2H, ArH), 7.18 – 7.14 (m, 2H, ArH), 6.96 (d, *J* = 8.1 Hz, 1H, ArH), 6.87 (d, *J* = 7.5 Hz, 1H, ArH), 4.61 – 4.59 (m, 2H, C_5H_4), 4.29 – 4.27 (m, 2H, C_5H_4), 4.00 (s, 5H, C_5H_5).^{13}C NMR (101 MHz, $CDCl_3$): δ 161.4, 161.2, 146.1, 138.7, 133.0, 132.2, 126.9, 121.3, 119.4, 119.1, 117.3, 84.5, 69.7, 69.2, 66.5. ESI-MS: *m/z* 382 $[M+H]^+$.

Ligand 3c

Reaction of 4-ferrocenyl aniline (277 mg, 1 mmol) and 4-diethylaminosalicylaldehyde (**2c**) (193.34 mg, 1 mmol) gave **3c** as an orange red crystalline solid, yield: 86%. ^{1}H NMR (400 MHz, $CDCl_3$): *δ* 13.92 (s, 1H, -OH), 8.45 (s, 1H, CH=N), 7.50 – 7.45 (m, 2H, Ar-H), 7.20 – 7.14 (m, 3H), 6.28 – 6.18 (m, 2H), 4.66 (s, 2H, C_5H_4), 4.33 (s, 2H, C_5H_4), 4.06 (s, 5H, C_5H_5), 3.40 (q, *J* = 7.1 Hz, 4H, CH_2), 1.21 (t, *J* = 7.1 Hz, 6H, CH_3). ^{13}C NMR (101 MHz, $CDCl_3$): *δ* 164.4, 159.4, 151.8, 146.4, 136.7, 133.7, 126.9, 120.8, 109.3, 103.8, 97.9, 85.1, 69.6, 69.0, 66.4, 44.6, 12.8. ESI-MS: *m/z* 453.3 $[M+H]^+$.

Ligand 3d

Reaction of 4-ferrocenyl aniline (277 mg, 1 mmol) and 4-methoxysalicylaldehyde (**2d**) (152.15 mg, 1 mmol) gave **3d** as an orange red crystalline solid, yield: 84%. ^{1}H NMR (300 MHz, $CDCl_3$): *δ* 13.92 (s, 1H, -OH), 8.58 (s, 1H, CH=N), 7.51 (d, *J* = 8.5 Hz, 2H, ArH), 7.30 (s, 1H, ArH), 7.21 (d, *J* = 8.4 Hz, 2H, ArH), 6.57 – 6.45 (m, 2H, ArH), 4.66 (s, *J* = 1.8 Hz, 2H, C_5H_4), 4.39 (s, 2H, C_5H_4), 4.06 (s, 5H, C_5H_5), 3.86 (s, 3H, OCH_3). ^{13}C NMR (126 MHz, $CDCl_3$): *δ* 164.1, 163.9, 160.3, 145.9, 137.9, 133.4, 126.9, 121.1, 113.3, 107.2, 101.2, 84.7, 69.7, 69.1, 66.5, 55.5. ESI-MS: *m/z* 412 $[M+H]^+$.

Ligand 3e

Reaction of 4-ferrocenyl aniline (277 mg, 1 mmol) and 5-bromosalicylaldehyde (**2e**) (201.02 mg, 1 mmol) gave **3e** as an orange red crystalline solid, yield: 81%. ^{1}H NMR (400 MHz, $CDCl_3$): *δ* 13.36 (s, 1H, -OH), 8.63 (s, 1H, CH=N), 7.53 (d, *J* = 7.5 Hz, 4H, ArH), 7.23 (d, *J* = 8.0 Hz, 2H, ArH), 6.89 (s, 1H, ArH), 4.68 (s, 2H, C_5H_4), 4.37 (s, 2H, C_5H_4), 4.07 (s, 5H, C_5H_5). ^{13}C NMR (101 MHz, $CDCl_3$): *δ* 160.2, 159.7, 145.3, 139.2, 135.5, 134.1, 127.0, 121.3, 120.8, 119.3, 110.5, 84.3, 69.7, 69.3, 66.6. ESI-MS: *m/z* 460 $[M+H]^+$.

Ligand 3f

Reaction of 4-ferrocenyl aniline (277 mg, 1 mmol) and 2-hydroxy-1-naphthaldehyde (**2f**) (172.05 mg, 1 mmol) gave **3f** as an orange red crystalline solid, yield: 87%. ^{1}H NMR (400 MHz, $CDCl_3$): *δ* 15.63 (s, 1H, -OH), 9.36 (d, *J* = 6.1 Hz, 2H), 8.11 (d, *J* = 8.4 Hz, 1H, CH=N), 7.80 (d, *J* = 9.2 Hz, 1H, ArH), 7.72 (d, *J* = 8.0 Hz, 1H, ArH), 7.58 – 7.52 (m, 3H, ArH), 7.37 – 7.29 (m, 3H, ArH), 7.09 (d, *J* = 9.2 Hz, 1H, ArH), 4.68 (s, 2H, C_5H_4), 4.39 (s, 2H, C_5H_4), 4.10 (s, 5H, C_5H_5). ^{13}C NMR (101 MHz, $CDCl_3$): *δ* 170.7, 153.5, 142.7, 138.2, 136.6, 133.3, 129.4, 128.1, 127.3, 127.2, 123.5, 122.5, 120.3, 118.9, 108.9, 84.4, 69.7, 69.3, 66.5. ESI-MS: *m/z* 432 $[M+H]^+$.

2.4 General procedure for the synthesis of complexes 5a-5f

Under a nitrogen atmosphere, a solution of **3a-3f** in dry ethanol (25 mL) was added to a two-neck round bottom flask equipped with magnetic stirrer and reflux condenser. Triethylamine was added dropwise to the solution, which was stirred at room temperature for 30 min. A solution of $[Ru(p\text{-cymene})Cl_2]_2$ in dry ethanol (5 mL) was added to the mixture and the reaction was heated to 70°C and stirred for 5 hours. The precipitated crude product and was isolated by filtration and purified by recrystallization from dichloromethane/hexane.

Complex 5a

Triethylamine (0.038 mL, 0.352 mmol) and ligand **3a** (150 mg, 0.352 mmol) were reacted with [Ru(*p*-cymene)Cl_2]$_2$ (107.7 mg, 0.176 mmol). The product **5a** was isolated as a black crystalline solid, yield: 78%. ^{1}H NMR (400 MHz, $CDCl_3$): δ 8.10 – 8.03 (m, 6H), 7.89 (s, 1H, CH=N), 7.58 – 7.50 (m, 12H), 6.95 (d, J = 9.4 Hz, 3H), 5.41 (d, J = 5.7 Hz, 3H), 5.33 (d, J = 5.5 Hz, 3H), 5.08 (d, J = 5.5 Hz, 3H), 4.73 – 4.69 (m, 6H), 4.42 – 4.39 (m, 6H), 4.31 (d, J = 5.9 Hz, 3H), 4.10 – 4.03 (s, 5H, Cp-H), 2.71 – 2.61 (m, 1H, 3^0-CH(η^6-*p*-cymene)), 2.17 (s, 3H, -CH_3 (η^6-*p*-cymene)), 1.19 (dd, J = 19.0, 6.9 Hz, 6H, CMe_2 (η^6-*p*-cymene)). ^{13}C NMR (101 MHz, $CDCl_3$): δ 170.3, 163.5, 155.7, 139.4, 135.9, 133.5, 129.6, 126.3, 123.2, 117.6, 102.4, 98.5, 86.6, 84.1, 83.6, 83.4, 81.3, 69.8, 69.6, 66.7, 66.5, 30.5, 22.8, 21.7, 18.6. Anal. Calcd. for $C_{33}H_{31}ClFeN_2O_3Ru$ (696.04): C 56.95, H 4.49, N 4.03%. Found: C 56.76, H 4.22, N 3.88%. MALDI-TOF MS: *m/z* 696.22 $[M]^+$.

Complex 5b

Triethylamine (0.056 mL, 0.524 mmol) and **3b** (200 mg, 0.524 mmol) were reacted with [Ru(*p*-cymene)Cl_2]$_2$ (160 mg, 0.262 mmol). The product was isolated as an orange crystalline solid, yield: 83%. H NMR (400 MHz, $CDCl_3$): δ 7.80 (s, 2H), 7.56 (dt, J = 18.9, 5.3 Hz, 8H), 7.26 – 7.19 (m, 2H), 7.02 – 6.95 (m, 4H), 6.46 – 6.41 (m, 2H), 5.35 (d, J = 6.1 Hz, 2H), 5.26 (d, J = 6.1 Hz, 2H), 5.04 (d, J = 5.7 Hz, 2H), 4.73 – 4.68 (m, 4H), 4.40 – 4.36 (m, 4H), 4.31 (d, J = 5.5 Hz, 2H), 4.09 (s, 5H), 2.64 (dq, J = 13.2, 6.6 Hz, 2H), 2.14 (s, 6H), 1.16 (dd, J = 19.8, 6.9 Hz, 12H). ^{13}C NMR (101 MHz, $CDCl_3$): δ 165.1, 163.9, 156.5, 138.4, 135.5, 135.3, 126.1, 123.8, 122.7, 118.3, 114.3, 101.5, 98.0, 86.4, 84.2, 83.6, 83.5, 80.6, 69.7, 69.4, 66.6, 66.5, 30.4, 22.9, 21.7, 18.6. Anal. Calcd. for $C_{33}H_{32}ClFeNORu$ (650.08): C 60.95, H 4.95, N 2.15%. Found: C 60.31, H 4.93, N 2.71%. MALDI-TOF MS: *m/z* 616.26 $[M\text{-}Cl]^+$.

Complex 5c

Triethylamine (0.035 mL, 0.331 mmol) and **3c** (150 mg, 0.331 mmol) were reacted with [Ru(*p*-cymene)Cl_2]$_2$ (101.57 mg, 0.165 mmol). The product was isolated as an orange red crystalline solid, yield: 85%. ^{1}H NMR (400 MHz, $CDCl_3$): δ 7.58 – 7.46 (m, 16H), 6.78 (d, J = 8.9 Hz, 3H), 6.22 (d, J = 2.1 Hz, 3H), 5.96 (dd, J = 8.9, 2.3 Hz, 3H), 5.31 (d, J = 6.0 Hz, 3H), 5.22 (d, J = 6.0 Hz, 3H), 5.01 (d, J = 5.4 Hz, 3H), 4.71 – 4.67 (m, 6H), 4.38 – 4.34 (m, 6H), 4.29 (d, J = 5.6 Hz, 3H), 4.10 – 4.05 (m, 14H), 3.39 – 3.29 (m, 12H), 2.66 (dt, J = 13.8, 6.9 Hz, 3H), 2.16 (s, 9H), 1.62 (s, 30H). ^{13}C NMR (101 MHz, $CDCl_3$): δ 160.7, 136.8, 126.0, 124.4, 102.4, 100.6, 100.3, 97.6, 86.3, 82.9, 80.6, 69.7, 69.2, 66.5, 44.4, 30.4, 22.9, 21.9, 18.6, 13.0. Anal. Calcd. for $C_{37}H_{41}ClFeNO_2Ru$ (722.13): C 61.54, H 5.72, N 3.88%. Found: C 60.85, H 5.52, N 3.50%. MALDI-TOF MS: *m/z* 687.32 $[M\text{-}Cl]^+$.

Complex 5d

Triethylamine (0.052 mL, 0.486 mmol) and **3d** (200 mg, 0.486 mmol) were reacted with [Ru(*p*-cymene)Cl_2]$_2$ (148.8 mg, 0.243 mmol). The product was isolated as an orange crystalline solid, yield: 83%. ^{1}H NMR (400 MHz, $CDCl_3$): δ 7.67 (s, 2H), 7.58 – 7.52 (m, 7H), 6.86 (d, J = 8.8 Hz, 2H), 6.49 (d, J = 2.0 Hz, 2H), 6.09 (dd, J = 8.7, 2.2 Hz, 2H), 5.29 (dd, J = 30.6, 6.1 Hz, 4H), 5.01 (d, J = 5.7 Hz, 2H), 4.70 (s, 4H), 4.37 (s, 4H), 4.28 (d, J = 5.6 Hz, 2H), 4.07 (s, 9H), 3.78 (s, 6H), 3.09 (q, J = 7.3 Hz, 4H), 2.66 (dt, J = 13.8, 6.8 Hz, 2H), 2.16 (s, 6H), 1.17 (dd, J = 17.3, 6.9 Hz, 12H). ^{13}C NMR (101 MHz, $CDCl_3$): δ 167.1, 166.1, 162.1, 156.8, 137.9, 136.5, 126.1, 124.0, 112.7, 105.8, 103.1, 101.0, 98.0, 86.5, 84.3, 83.3, 83.2, 80.8, 69.7, 69.3, 66.5, 66.4, 55.2, 45.9, 30.4, 22.9, 21.7, 18.6, 8.7. Anal. Calcd. for $C_{34}H_{34}ClFeNO_2Ru$ (681.01): C 59.96, H 5.03, N 2.06%. Found: C 59.47, H 5.24, N 2.17%. MALDI-TOF MS: *m/z* 646.22 $[M\text{-}Cl]^+$.

Complex 5e

Triethylamine (0.035 mL, 0.325 mmol) and **3e** (150 mg, 0.325 mmol) were reacted with [Ru(*p*-cymene)Cl_2]$_2$ (99.73 mg, 0.162 mmol). The product was isolated as an orange-red crystalline solid, yield: 79%. ^{1}H NMR (500 MHz, $CDCl_3$): δ 7.72 (s, 1H), 7.54 (s, 4H), 7.26

– 7.21 (m, 1H), 7.08 (d, *J* = 2.6 Hz, 1H), 6.89 (d, *J* = 9.2 Hz, 1H), 5.35 (d, *J* = 6.1 Hz, 1H), 5.27 (d, *J* = 6.1 Hz, 1H), 5.02 (d, *J* = 5.7 Hz, 1H), 4.72 – 4.68 (m, 2H), 4.41 – 4.37 (m, 2H), 4.27 (d, *J* = 5.7 Hz, 1H), 4.07 (d, *J* = 6.8 Hz, 5H), 3.10 (d, *J* = 7.1 Hz, 1H), 2.64 (sept, *J* = 6.9 Hz, 1H), 2.15 (s, 3H), 1.17 (dd, *J* = 24.9, 6.9 Hz, 6H). ^{13}C NMR (126 MHz, $CDCl_3$): *δ* 164.2, 162.8, 156.2, 138.8, 138.0, 136.5, 126.1, 124.7, 123.5, 119.8, 104.9, 101.6, 98.2, 86.6, 88.0, 83.7, 83.5, 80.8, 69.8, 69.5, 66.6, 66.5, 30.4, 29.7, 22.9, 21.7, 18.6. Anal. Calcd. for $C_{33}H_{31}BrClFeNORu$ (728.97): C 54.30, H 4.28, N 1.92%. Found: C 54.35, H 4.63, N 2.00%. MALDI-TOF MS: *m*/*z* 694.13$[M\text{-}Cl]^+$.

Complex 5f

Triethylamine (0.040 mL, 0.371 mmol) and **3f** (160 mg, 0.371 mmol) were reacted with $[Ru(p\text{-cymene})Cl_2]_2$ (113.6 mg, 0.185 mmol). The product was isolated as a maroon crystalline solid, yield: 80%. ^{1}H NMR (500 MHz, $CDCl_3$): *δ* 8.64 (s, 1H), 7.75 (d, *J* = 8.2 Hz, 1H), 7.58 (dd, *J* = 25.4, 7.4 Hz, 6H), 7.33 (t, *J* = 7.2 Hz, 1H), 7.21 – 7.11 (m, 2H), 5.35 (d, *J* = 38.2 Hz, 2H), 5.03 (d, *J* = 4.8 Hz, 1H), 4.73 (s, 2H), 4.40 (s, 2H), 4.32 (d, *J* = 4.7 Hz, 1H), 4.09 (d, *J* = 16.3 Hz, 5H), 3.72 (s, 1H), 2.71 – 2.60 (m, 1H), 2.17 (s, 3H), 1.16 (dd, *J* = 33.1, 6.6 Hz, 6H). ^{13}C NMR (101 MHz, $CDCl_3$): *δ* 166.1, 157.5 (d, *J* = 25.8 Hz), 138.0, 135.8, 134.9, 128.9, 127.3, 126.7, 126.2, 125.5, 124.3, 121.9, 118.7, 108.3, 101.4, 98.0, 86.5, 84.3, 83.8, 80.8, 69.8, 69.6 (d, *J* = 41.4 Hz), 66.6, 30.5, 22.9, 21.7, 18.6. Anal. Calcd. for $C_{37}H_{34}ClFeNORu$ (701.07): C 63.39, H 4.89, N 2.00%. Found: 62.94, H 4.14, N 1.82%. MALDI-TOF MS: *m*/*z* 666.22 $[M\text{-}Cl]^+$.

2.5. Electrochemistry

Cyclic voltammetry (CV) and differential pulse voltammetry (DPV) were performed using CH instruments model 620C series, using a conventional three-electrode cell consisting of a glassy carbon working electrode, a platinum wire auxiliary electrode and a standard calomel electrode (SCE) as the reference electrode with a scan rate of 100 mV s^{-1}. All the experiments were carried out by dissolving the ligands and complexes in CH_3CN (1.0 mM) containing 0.1 M $[n\text{-}Bu_4N]ClO_4$ as supporting electrolyte. All potentials are relative to the ferrocene/ferrocenium couple. Deoxygenation of all solutions was achieved by purging with nitrogen gas for 5 minutes prior to analysis.

2.6 X- Ray diffraction studies

Orange crystals of **3e** were obtained from the slow evaporation of a dichloromethane-hexane (9:1) solution and maroon colored crystals of **5f** were obtained by the slow evaporation of a dichloromethane-methanol (9:1) solution. Data for compounds **3e** (at room temperature) and **5f** (at 100 K) were collected on a Bruker D8 QUEST diffractometer with a 1 μS Mo microsource (λ = 0.7107 Å) and a PHOTON-100 detector. The raw data frames were reduced and corrected for absorption effects using the Bruker Apex 3 software suite of programs. The structures were solved using the intrinsic phasing method and further refined with the SHELXL[21] program and expanded using Fourier techniques. Anisotropic displacement parameters were included for all non-hydrogen atoms. All C bound H atoms were positioned geometrically and treated as riding on their parent C atoms [C-H = 0.93-0.97 Å and $U_{iso}(H) = 1.5U_{eq}(C)$ for methyl H or $1.2U_{eq}(C)$ for other H atoms]. The dichloromethane solvent molecule of **5f** could not be resolved due to extensive disorder and its assumed presence was removed from the overall scattering by the PLATON SQUEEZE procedure. The computer program OLEX2 was used to generate the X-ray crystal structure images.[22]

Journal Pre-proofs

Crystal Data for 3e $C_{23}H_{18}NOFeBr$ (*M* = 460.15 g/mol): monoclinic, space group $P2_1/c$ (no. 14), *a* = 22.6635(4) Å, *b* = 7.3233(9) Å, *c* = 11.8142(2) Å, β = 102.8624(5)°, *V* = 1911.6(2) $Å^3$, *Z* = 4, *T* = 293.15 K, μ(Mo Kα) = 2.891 mm^{-1}, *Dcalc* = 1.5987 g/cm^3, 38785 reflections measured ($5.54 \leq 2\Theta \leq 55.1$), 4400 unique ($R_{int}$ = 0.0277, R_{sigma} = 0.0176) which were used in all calculations. The final R_1 was 0.0449 (≥2u(I)) and wR_2 was 0.1111 (all data). CCDC 1818439 contains the supplementary crystallographic data for the structure.

Crystal Data for 5f

$C_{38}H_{36}Cl_2FeNORu$ (*M* = 750.50 g/mol): monoclinic, space group $P2_1/n$ (no. 14), *a* = 16.0789(2) Å, *b* = 9.75390(10) Å, *c* = 20.1984(2) Å, β = 101.0720(5), *V* = 3108.79(6) $Å^3$, *Z* = 4, *T* = 100.09 K, μ(MoKα) = 1.158 mm^{-1}, *Dcalc* = 1.603 g/cm^3, 67265 reflections measured ($4.654 \leq 2\Theta \leq 56.694$), 7728 unique (R_{int} = 0.0383, R_{sigma} = 0.0227) which were used in all calculations. The final R_1 was 0.0332 ($I > 2\sigma(I)$) and wR_2 was 0.0830 (all data). CCDC 1818440 contains the supplementary crystallographic data for the structure. These data can be obtained free of charge at www.ccdc.cam.ac.uk/conts/retrieving.html [or from the Cambridge Crystallographic Data Centre (CCDC), 12 Union Road, Cambridge CB2 1EZ, UK; fax: +44(0) 1223 336 033; email: deposit@ccdc.cam.ac.uk].

2.7 *In vitro* anti-cancer activity

HepG2 human liver cancer cells and HeLa human cervical cancer cells were cultured in DMEM medium supplemented with 10% FBS, 2 mM glutamine, penicillin (100 U/mL) and streptomycin (0.1 mg/mL) in a CO_2 incubator (5% CO_2, 37 °C). The anti-cancer activity of the compounds were assessed using the MTT assay. Stock solutions of the compounds were prepared in DMSO (10 mM). Cells (5×10^3) were seeded in 96-well culture plates and allowed to adhere overnight at 37 °C. The cells were then incubated with varying concentrations (0.01-100 μM) of the compounds. The concentration of DMSO did not exceed 1% in the treatment wells. After 48 h, the media was replaced with fresh media (containing 0.5 mg/mL MTT) and the cells were further incubated for 4 h. The media was removed and 150 μL of DMSO was added to dissolve the formazan crystals. The absorbance of the solution was measured at 570 nm using a micro-plate reader (Synergy-4, Biotek, USA). Untreated cells were used as a negative control (100% cell viability). The percent cell viability was calculated using the formula

% Cell viability = As/Ac × 100%,

where, As = absorbance of the sample and Ac = absorbance of the control or untreated cells, incubated under identical conditions. The half-maximal inhibitory concentration (IC_{50}) values were determined using the probit analysis software package of MS-excel. Data are expressed as the average ± the standard deviation (n = 4).

Cell Cycle analysis

HepG2 cells were seeded in a 6 well plate at cell densities of 1×10^5 cells/well and incubated overnight. The cells were treated with various concentrations (10, 15 and 20 μM) of compound **5d** for 48 h. After the treatment, the cells were harvested using 0.05% trypsin-EDTA and washed with phosphate buffered saline. Then, the cells were fixed with 70% cold ethanol and incubated at 4 °C for 30 min. The fixed cells were washed with PBS and stained with propidium iodide staining buffer [PI (20 μg/mL), 0.01 % Triton X] containing 200 μg/mL DNase free RNase A and incubated in the dark for 30 min. The DNA content of the cells in each phase of the cell cycle was analyzed from 10000 events in each sample using a BDC6-Accuri flow cytometer.

Assessment of mitochondrial membrane potential

HepG2 cells seeded in a 24 well plate were incubated with various concentrations (10, 15 and 20 μM) of compound **5d** for 48 h. Rhodamine 123 solution was added to cells and incubated

for 30 min. The medium containing the drug and dye was removed and the cells were washed with PBS. The cells were harvested and washed with PBS and the fluorescence intensity was determined using a plate reader.

Reactive oxygen species

HepG2 cells were plated in a 24 well plate at a density of 3×10^4 cells/mL and incubated overnight. The cells were then treated with different concentrations (10, 15 and 20 µM) of compound **5d** and incubated for 48 h. Carboxy-DCFHDA (5 mM) solution was added to the cells to give a final concentration of 10 µM in each well 30 min prior to the termination of the experiment. At the end of the experiment, the medium was replaced with fresh complete medium and the cells were incubated for a further 30 min in a humidified atmosphere at 37 °C. Images were captured using a BIORAD microscope.

3.0 Results

3.1 Synthesis and characterization

p-Ferrocenyl aniline **1** was synthesized according to a literature method by the diazotization of 4-nitroaniline followed by reaction with ferrocene and subsequent reduction of the nitro group using Sn/HCl.[23] Through a typical Schiff-base condensation reaction, **1** was reacted with the aldehyde **2a-2f** to afford the corresponding ferrocenyl phenyl salicylaldimine ligands **3a-3f** (Scheme 1), which were subsequently treated with [Ru(*p*-cymene)Cl_2]$_2$ in the presence of triethylamine to give the desired Ru-Fe complexes **5a-5f** (Scheme 2).

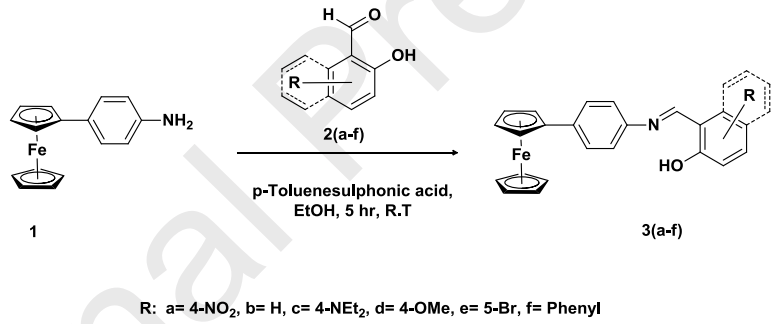

Scheme 1. Synthesis of ferrocenyl Schiff base ligands **3a-3f**.

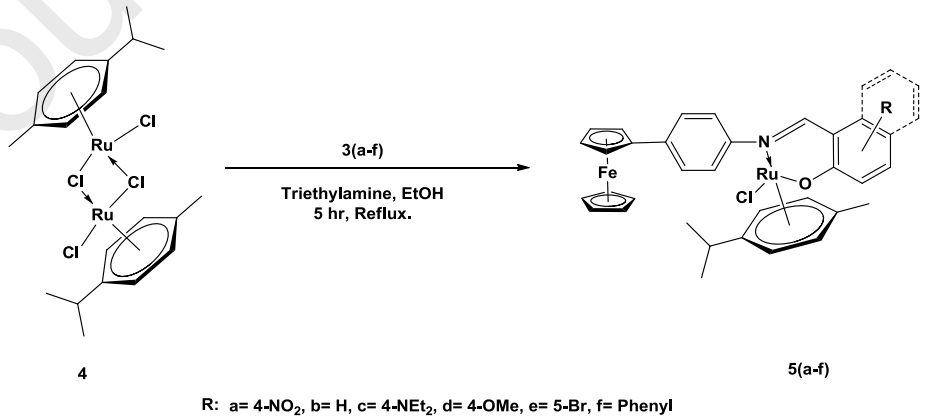

Scheme 2. Synthesis of hetero-bimetallic Ru-Fe complexes **5a-5f**.

The ^{1}H NMR spectra for the ligands **3a-3f** and complexes **5a-5f** revealed the expected resonances for the ferrocenyl moiety. The proton signals for the unsubstituted cyclopentadienyl ring appeared as a singlet at δ 4.28 ppm. The resonances for the protons of the substituted cyclopentadienyl ring appeared as broadened singlets at δ 4.55 ppm and 4.78 ppm. Typically, the protons on the substituted ring of the ferrocenyl moieties that contain a monosubstituted Cp ring appear as a doublet or triplet.[24] The resonances for the aromatic protons on the phenyl ring attached to the ferrocenyl moiety appeared around δ 6.5-7.5 ppm. In the ligands **3a-3f**, the –OH protons appeared in the range δ 13.3-15.6 and the presence of a signal at around δ 8.23-8.86 ppm was assigned to the imine proton (Supporting Information). The formation of the ruthenium complexes **5a-5f** was indicated by the disappearance of the phenolic –OH resonance and an upfield shift of the imine proton resonance to about δ 7.31-7.74 ppm (Supporting Information). In the ^{13}C NMR spectra of the ligands and complexes, the characteristic peaks associated with the substituted and unsubstituted cyclopentadienyl rings of the ferrocenyl moiety were observed in the range δ 69.53-71.58 ppm and at δ 69.07 ppm, respectively. The imine carbon resonances appeared around δ 162-166. In the infrared spectrum, the imine stretching bands were typically observed in the range 1580-1650 cm^{-1}. For the complexes, the imine vibration of the salicylaldimine moiety was observed around 1619 cm^{-1} while the band for the ferrocenyl imine moiety appeared around 1585 cm^{-1} (Supporting Information, Figures S37-S46). In the ESI mass spectra of **3a-3f**, peaks corresponding to the $[M+H]^+$ ions were observed. The MALDI-TOF mass spectra of complexes **5b-5f** showed peaks corresponding to the $[M–Cl]^+$ fragments, whereas **5a** showed the $[M]^+$ parent ion, confirming the formation of the expected ruthenium(II) complexes.

The molecular structures of the ligand **3e** and the complex **5f** were determined by X-ray diffraction and are shown in Figures 3 and 4, respectively. Selected bond angles and bond lengths for **3e** and **5f** are summarized in Table S4 (Supporting Information). The compounds **3e** and **5f** crystallized in the monoclinic $P2_1/c$ and $P2_1/n$ space groups, respectively. The molecular structure of **5f** reveals the orientation of the ferrocene group and ruthenium η^6-*p*-cymene with respect to the salicylaldimine moiety. The ruthenium atom is coordinated by the imine nitrogen atom (N1), phenolic oxygen atom (O1), chlorine atom (Cl1) and the *p*-cymene ring to adopt the typical distorted piano-stool geometry.[25] The Ru-O [2.0566(16) Å] and Ru-N [2.0767(18) Å] bond lengths are typical for Ru(II) half-sandwich complexes containing *N,O* ligands.[26]

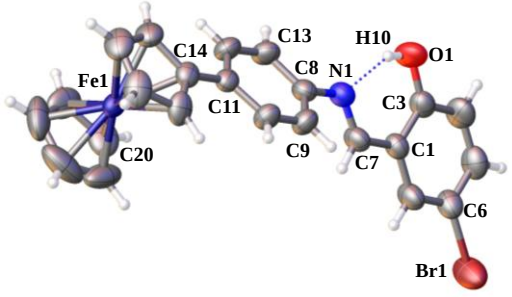

Figure 3. Molecular structure of **3e**. Ellipsoids show 50% probability levels. The intramolecular hydrogen bond is shown as a dashed line.

Journal Pre-proofs

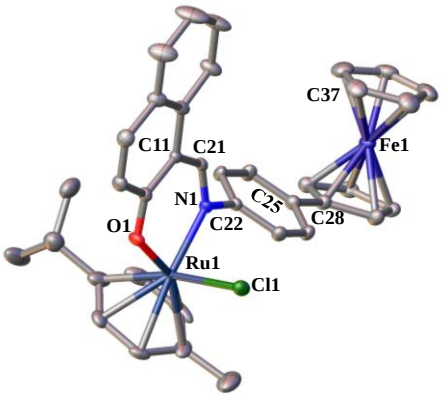

Figure 4. Molecular structure of **5f**. Ellipsoids show 50% probability levels. Hydrogen atoms and disordered CH_2Cl_2 solvent of crystallization have been omitted for clarity.

3.2 UV-vis. spectroscopy

The UV-vis. absorption spectra (Figure 5) of the ligands and complexes in acetonitrile displayed bands corresponding to n–π* and π–π* transitions. The stronger and higher energy bands were attributed to the π–π* transition of the Schiff base in **3a-3f** and **5a-5f** due to symmetry allowed transitions of the phenyl rings while the less energetic bands were assigned to n–π* transitions.[27] The bands at 295 and 445 nm are typical of Fe(e_{2g}) → Cp(e_{1g}) charge transfer and symmetry forbidden Fe(a_{1g}) → Fe(e_{1g}) transitions, respectively. The ligands **3b**, **3d** and **3e** exhibited absorption maxima at around 355 nm, while ligand **3a** showed a shoulder peak at 285 nm due to the strong electron withdrawing effect of the nitro group. For ligands **3c** and **3f**, the absorption maxima appeared at 400 nm. The complexes **5a**, **5b**, **5d-5f** exhibited two absorption maxima at around 295 and 445 nm. In contrast, the spectrum for **5c** showed a band at 365 nm due to the presence of the strongly electron donating diethylamino group (Supporting Information, Figures S47-S48).

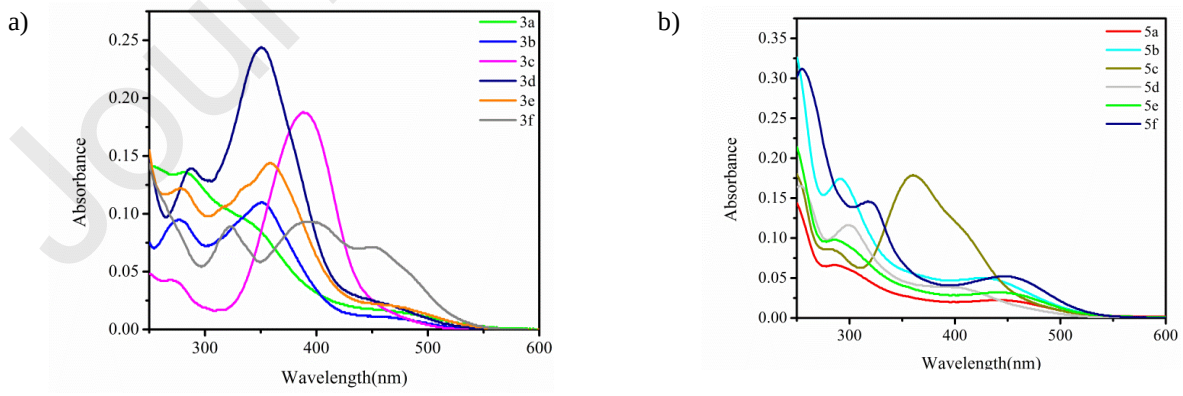

Figure 5. UV-vis. spectra of 0.6×10^{-5} M solutions of a) ligands **3a-3f** and b) complexes **5a-5f** in acetonitrile at 25 °C.

3.3 Electrochemical studies

Journal Pre-proofs

The electrochemical properties of **3a-3f** and **5a-5f** were studied in acetonitrile by cyclic voltammetry (CV) and differential pulse voltammetry (DPV). The cyclic and differential pulse voltammograms of the compounds are shown in the Supporting Information (Figures S49 and S50, respectively). In the CV, a reversible oxidation wave at 0.4 V was observed for **3a-3f** and **5a-5f** due to the [Fe(II) → Fe(III)] ferrocenyl oxidation wave, as shown in Figure 6 for selected examples. An irreversible oxidation wave for complexes **5a-5f** due to the [Ru(II) → Ru(III)] oxidation of the ruthenium center appeared in the region of 0.75 to 0.9 V. Similarly, based on the electron donating/withdrawing substituents on the ligands, other irreversible oxidation potentials were observed, as shown in Tables S1 and S2 (Supporting Information). According to existing literature, facile oxidation of the ferrocenyl moiety in the complexes can produce reactive oxygen species that disrupt lipid membranes and in turn influence the anti-tumor activity of the complexes.[10] This phenomenon is in agreement with the results found for complexes **5a-5f**.

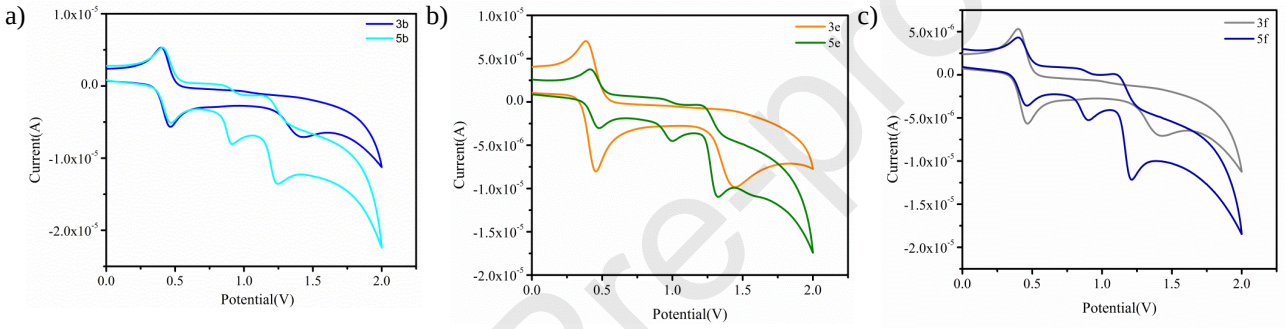

Figure 6. Cyclic voltammograms of a) **3b**, **5b**, b) **3e**, **5e** and c) **3f**, **5f** in acetonitrile solution at 25 °C with 0.1 M tetrabutylammonium perchlorate as a supporting electrolyte using a SCE reference electrode, glassy carbon working electrode and platinum wire counter electrode.

3.4 *In vitro* anti-cancer activity

The antiproliferative activities of **3a-3f** and **5a-5f** were evaluated against two different cancer cell lines, human cervical carcinoma (HeLa) and human liver carcinoma (HepG2) using the MTT assay.[28] The cell viability after treatment with the compounds at different concentrations for both cell lines are shown in Figure 7 and compared to cisplatin as a standard. The calculated IC_{50} are shown in Table 1. All the complexes exhibited moderate to high cytotoxicity towards both HeLa and HepG2 cancer cell lines with low IC_{50} values. With the exception of **5c**, all the tested compounds showed greater sensitivity towards HepG2 cells than HeLa cells. Enhanced cytotoxicity was observed against both cell lines for the ruthenium-containing complexes **5a-5f** compared to the ferrocenyl compounds **3a-3f**. Exceptionally, the bromo-substituted ferrocenyl salicylaldimine **3e** exhibited significant cytotoxicity (IC_{50}, 18.29±1.47 µM) against HepG2 cells. For the HepG2 cell line, compound **5d** showed the greatest cytotoxicity (IC_{50}, 15.74±2.63 µM) among all the complexes, including the standard (cisplatin, IC_{50}, 27.93±3.15 µM). Interestingly, complex **5c** exhibited the most greatest cytotoxicity against HeLa cells with IC_{50} 9.34±1.23 µM and was 3.3 times more cytotoxic than cisplatin (IC_{50}, 31.32±3.47 µM).

Table 1 IC_{50} values of different complexes against HeLa and HepG2 cell lines determined using the MTT assay (n = 4, ± SD).

Test compound	Metal	IC_{50} (μM)[a]		Test compound	Metal	IC_{50} (μM)	
		HeLa	HepG2			HeLa	HepG2
3a	Fe	96.73±7.52	67.73±5.32	**5a**	Ru-Fe	137.74± 8.72	43.97 ±4.42
3b	Fe	84.84±7.22	37.73±5.33	**5b**	Ru-Fe	29.91± 2.56	17.88± 3.56
3c	Fe	488.55±14.63	52.08±3.65	**5c**	Ru-Fe	9.34 ±1.23	38.37± 4.12
3d	Fe	252.44±11.87	64.96±4.85	**5d**	Ru-Fe	21.08± 1.98	15.74 ±2.63
3e	Fe	50.28±4.74	18.29±1.47	**5e**	Ru-Fe	25.36 ±3.89	21.90 ±2.85
3f	Fe	127.22 ±14.23	30.58± 2.85	**5f**	Ru-Fe	137.81± 7.56	30.73 ±3.96
Cisplatin	Pt	31.32 ±3.47	27.95± 3.15	**Cisplatin**	Pt	31.32 ±3.47	27.95± 3.15

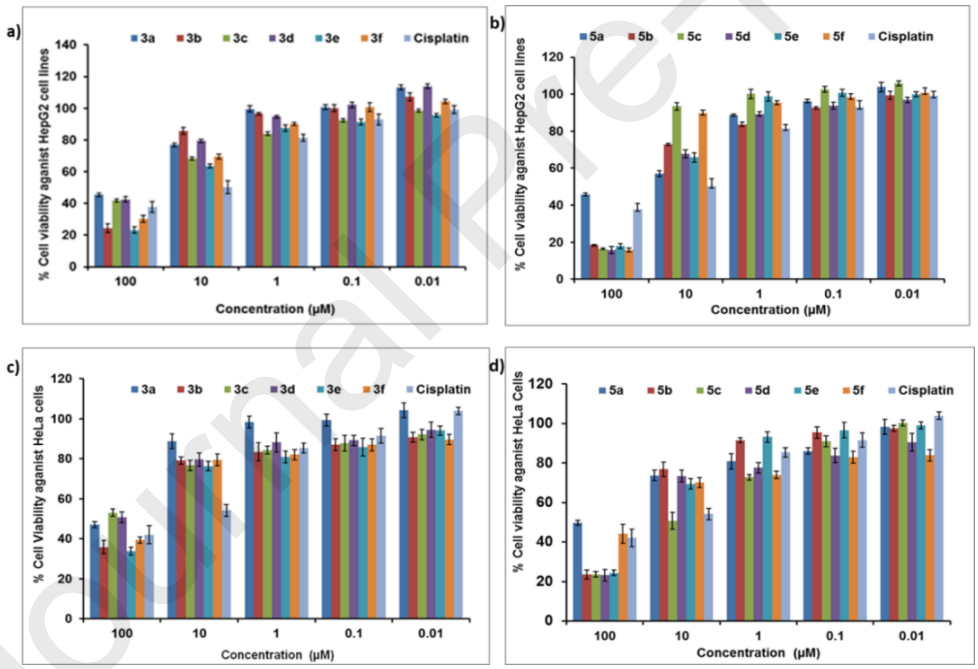

Figure 7. Percentage cell viability of HepG2 human liver carcinoma cells (a and b) and HeLa human cervical cancer cells (c and d) after treatment with varying concentration of ligands **3a-3f** (left) and complexes **5a-5f** (right) (mean ± SD, n = 4). Untreated cells were taken as control.

3.5 Cell cycle analysis

Considering the cytotoxicity results of complexes **5a-5f** towards cervical and liver cancer cells, compound **5d** was selected to further investigate the mechanism of cell growth inhibition in liver cancer cells. In order to investigate whether compound **5d** induces cell cycle arrest in HepG2 cells, flow cytometric analysis was carried out after 48 h of treatment with various concentrations of the compound.[29] As shown in Figure 8, compound treatment

resulted in a dose dependent increase in apoptotic cells (Sub G1 cells). The percentage of cells undergoing apoptosis increased remarkably at 15 and 20 µM (10.4 and 15.6%) compared to untreated cells (1.3%). Similarly, the number of cells in the S phase increased significantly in a concentration dependent manner from 13.2 to 35.5%. These results indicate that compound **5d** induces cell cycle arrest in the Sub G1 and S phases in HepG2 cells.

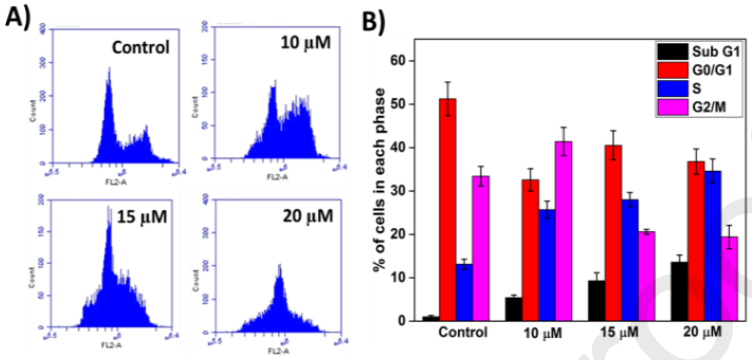

Figure 8. Cell cycle analysis of HepG2 cells. A) The cells were treated with various concentrations (10, 15 and 20 µM) of the compound **5d** and were stained with propidium iodide. The samples were analyzed using flow cytometry. B) Histogram showing the percentage of cells in each phase of the cell cycle. The results are expressed as the mean ± standard deviation of three independent experiments.

3.6 Mitochondrial membrane potential

The depolarization of mitochondrial membrane potential (ΔΨ m) is considered an early event that occurs during apoptosis.[30] Therefore, we measured the changes in mitochondrial membrane potential (Ψm) to determine the possible mechanism of apoptosis induction by compound **5d** using rhodamine-123 (Rh123), which is a fluorescent probe specific for the detection of alterations in ΔΨm in living cells.[31] HepG2 cells incubated with various concentrations of compound **5d** were stained with Rh123 and the fluorescence intensity of Rh123 in mitochondria was analyzed by spectrophotometry. The results, shown in Figure 9, demonstrated that compound **5d** treatment resulted in a 13.4 to 31.6% reduction in fluorescence intensity, corresponding to a decrease in mitochondrial membrane potential. The loss of ΔΨm was found to be 13.4, 22.5 and 31.6% at concentrations of 10, 15 and 20 µM, respectively. These results suggest that compound **5d** could induce apoptosis through disruption of mitochondrial membrane potential in HepG2 cells.

Journal Pre-proofs

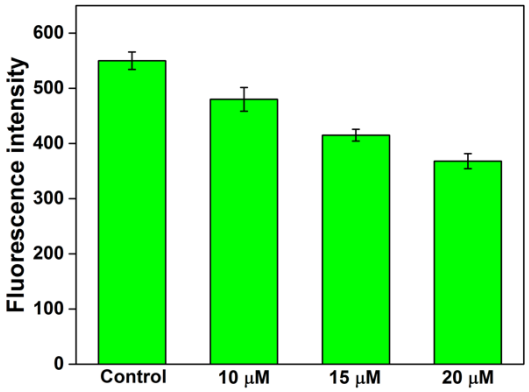

Figure 9. Effect of compound **5d** on intracellular mitochondrial membrane potential. The image shows graphically the decrease in fluorescence intensity of mitochondrial specific dye Rh 123 with increasing concentration of **5d** compared to control. The results are expressed as the mean ± standard deviation of three independent experiments.

3.7 Reactive oxygen species (ROS)

It has been reported that disruption of mitochondrial membrane potential leads to increased ROS production.[32] Therefore, to investigate whether this event occurred in HepG2 cells treated with compound **5d**, we used the oxidation-sensitive membrane permeable probe 2′,7′-dichlorofluorescein diacetate (DCFH-DA).[33] As shown in Figure 10, the incubation of HepG2 cells with various concentrations of compound **5d** significantly increased ROS levels, as indicated by the increased DCF fluorescence. For instance, 6- and 16-fold increased ROS accumulation relative to the control was observed after treatment with 15 and 20 μM of compound **5d** for 48 h. These results illustrate that compound **5d** treatment led to increased intracellular ROS levels in a dose dependent manner.

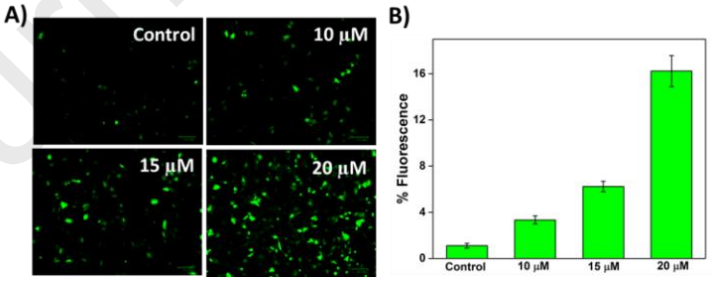

Figure 10. Impact of compound **5d** on intracellular ROS in HepG2 cells. A) HepG2 cells were treated with different concentrations (10, 15 and 20 μM) of compound **5d** and stained with carboxy-DCFH-DA. The images were captured with a BIORAD microscope. B) Quantification of the green fluorescence was carried out using software imageJ.

4.0 Conclusion

The synthesis and characterization of half-sandwich ruthenium η^6-*p*-cymene complexes containing ferrocenyl salicylaldimine ligands are described. All the compounds exhibited

good to moderate cytotoxicity towards HeLa and HepG2 cells. Complexes containing strong donor groups on the salicylaldehyde ligands, such as diethylamino (NEt_2) and methoxy (OMe), displayed cell-specific activity. In particular, compounds **5c** and **5d** showed promising anti-cancer activity against HeLa cancer cells (IC_{50} values of 9.34 and 21.08 μM, respectively) and HepG2 cancer cells (IC_{50} values of 38.37 and 15.74 μM, respectively) which were found to be among the best IC_{50} values reported for ferrocenyl-ruthenium complexes. Mechanistic studies indicated that compound **5d** arrests the HepG2 cells in the S phase of the cell cycle. Compound **5d** also induces apoptosis through mitochondrial membrane disruption and increased ROS. These results indicate the importance of the salicylaldehyde derived scaffolds in designing ferrocenyl-ruthenium complexes, hence the present work describes a simple approach towards the development of ruthenium-based imines containing ferrocenyl derivatives. Further experiments involving the study of structural modifications and other biological studies to determine the role of these compounds on the apoptotic and proliferative pathways in tumor lines are in progress.

Acknowledgements

This work was financially supported by the CSIR-IICT (in-house project MLP-0007) and DST-(EMR/2016/006410). ERR acknowledges DST-SERB, India for the SERB-NPDF (PDF/2016/003495) and AKV acknowledges SERB-NPDF (PDF/2016/001158). JRK is grateful to the IICT-RMIT Centre for the award of a research fellowship. We also thank the Director, CSIR-IICT (Ms. No. 11CT/Pubs/2020/103).

References

[1] B. Rosenberg, L. Van Camp, T.J.N. Krigas, Nature 205 (1965) 698-699.

[2] B. Rosenberg, L. Vancamp, J.E. Trosko, V.H. Mansour, Nature 222 (1969) 385-386.

[3] E.R. Jamieson, S.J. Lippard, Chem. Rev. 99 (1999) 2467-2498.

[4] a) P.-S. Kuhn, V. Pichler, A. Roller, M. Hejl, M. A. Jakupec, W. Kandioller, B.K. Keppler, Dalton Trans. 44 (2015) 659-668. b) S.W. Chang, A.R. Lewis, K.E. Prosser, J.R. Thompson, M. Gladkikh, M.B. Bally, J.J. Warren, C.J. Walsby, Inorg. Chem. 55 (2016) 4850-4863. c) S. Thota, D.A. Rodrigues, D.C. Crans, E.J. Barreiro, J. Med. Chem .61 (2018) 5805-5821.

[5] a) B.S. Murray, M.V. Babak, C.G. Hartinger, P.J. Dyson, Coord. Chem. Rev. 306 (2016) 86-114. b) S. Chatterjee, S. Kundu, A. Bhattacharyya, C.G. Hartinger, P.J. Dyson, J. Biol. Inorg. Chem. 13 (2008) 1149. c) P. Govender, L.C. Sudding, C.M. Clavel, P.J. Dyson, B. Therrien, G.S. Smith, Dalton Trans. 42 (2013) 1267-1277.

[6] a) L. Zeng, P. Gupta, Y. Chen, E. Wang, L. Ji, H. Chao, Z.-S. Chen, Chem. Soc. Rev. 46 (2017) 5771-5804. b) G. Palermo, A. Magistrato, T. Riedel, T. Von Erlach, C.A. Davey, P.J. Dyson, U. Rothlisberger, Chem. Med. Chem 11 (2016) 1199-1210.

Journal Pre-proofs

[7] R. Fernández, M. Melchart, A. Habtemariam, S. Parsons, P.J. Sadler, Chem. Eur. J. 10 (2004) 5173-5179.

[8] A. Habtemariam, M. Melchart, R. Fernández, S. Parsons, I.D.H. Oswald, A. Parkin, F.P.A. Fabbiani, J.E. Davidson, A. Dawson, R.E. Aird, D.I. Jodrell, P.J. Sadler, J. Med. Chem. 49 (2006) 6858-6868.

[9] a) T.C. Johnstone, K. Suntharalingam, S.J. Lippard, Chem. Rev. 116 (2016) 3436-3486. b) J. Reedijk, Inorg. Chim. Acta 198 (1992) 873-881.

[10] a) P. Govender, N.C. Antonels, J. Mattsson, A.K. Renfrew, P.J. Dyson, J.R. Moss, B. Therrien, G.S. Smith, J. Organomet. Chem. 694 (2009) 3470-3476. b) P. Govender, A.K. Renfrew, C.M. Clavel, P.J. Dyson, B. Therrien, G.S. Smith, Dalton Trans. 40 (2011) 1158-1167. c) F. Chen, I. Romero-Canelón, J.J. Soldevila-Barreda, J.-I. Song, J.P.C. Coverdale, G.J. Clarkson, J. Kasparkova, A. Habtemariam, M. Wills, V. Brabec, P.J. Sadler, Organometallics 37 (2018) 1555-1566. d) J. Zhao, D. Zhang, W. Hua, W. Li, G. Xu, S. Gou, Organometallics 37 (2018) 441-447.

[11] H. Chen, J.A. Parkinson, R.E. Morris, P.J. Sadler, J. Am. Chem. Soc. 125 (2003) 173-186.

[12] a) W. Nkoana, D. Nyoni, P. Chellan, T. Stringer, D. Taylor, P.J. Smith, A.T. Hutton, G.S. Smith, J. Organomet. Chem. 752 (2014) 67-75. b) M. Auzias, J. Gueniat, B. Therrien, G. Süss-Fink, A.K. Renfrew, P.J. Dyson, J. Organomet. Chem. 694 (2009) 855-861.

[13] a) K. Heinze, H. Lang, Organometallics 32 (2013) 5623-5625. b) C. Ornelas, New J. Chem. 35 (2011) 1973-1985.

[14] P. Govender, H. Lemmerhirt, A.T. Hutton, B. Therrien, P.J. Bednarski, G.S. Smith, Organometallics 33 (2014) 5535-5545.

[15] a) D. Osella, M. Ferrali, P. Zanello, F. Laschi, M. Fontani, C. Nervi, G. Cavigiolio, Inorg. Chim. Acta 306 (2000) 42-48. b) G. Tabbì, C. Cassino, G. Cavigiolio, D. Colangelo, A. Ghiglia, I. Viano, D. Osella, J. Med. Chem. 45 (2002) 5786-5796.

[16] a) I. Romero-Canelon, P.J. Sadler, Inorg. Chem. 52 (2013) 12276-12291. b) E. Reisner, V.B. Arion, B.K. Keppler, A.J.L. Pombeiro, Inorg. Chim. Acta. 361 (2008) 1569-1583. c) P. Zhang, P.J. Sadler, Eur. J. Inorg. Chem. (2017) 1541-1548.

[17] a) N. Lease, V. Vasilevski, M. Carreira, A. de Almeida, M. Sanaú, P. Hirva, A. Casini, M. Contel, J. Med. Chem. 56 (2013) 5806-5818. b) J. Rajput, J.R. Moss, A.T. Hutton, D.T. Hendricks, C.E. Arendse, C. Imrie, J. Organomet. Chem. 689 (2004) 1553-1568. c) X. Ge, S. Chen, X. Liu, Q. Wang, L. Gao, C. Zhao, L. Zhang, M. Shao, X.-A. Yuan, L. Tian, Z. Liu, Inorg. Chem. 58 (2019) 14175-14184. d) F. Du, L. Bai, M. He, W.-Y. Zhang, Y.-Y. Gu, H. Yin, Y.-J. Liu, J. Inorg. Biochem. 201 (2019) 110822. e) J. Li, Z. Tian, X. Ge, Z. Xu, Y. Feng, Z. Liu, Eur. J. Med. Chem. 163 (2019) 830-839.

[18] a) M. Auzias, B. Therrien, G. Süss-Fink, P. Stepnicka, W.H. Ang, P.J. Dyson, Inorg. Chem. 47 (2008) 578-583. b) H. Charvátová, T. Riedel, I. Císařová, P.J. Dyson, P. Stepnicka, J. Organomet. Chem. 802 (2016) 21-26.

Journal Pre-proofs

[19] P. Ramadevi, R. Singh, S.S. Jana, R. Devkar, D. Chakraborty, J. Organomet. Chem. 833 (2017) 80-87.

[20] a) S. Acharya, M. Maji, Ruturaj, K. Purkait, A. Gupta, A. Mukherjee, Inorg. Chem. 58 (2019) 9213-9224. b) K.S. Neethu, E. Jayanthi, M. Theetharappan, N.S.P. Bhuvanesh, M.A. Neelakantan, M.V Kaveri, Appl. Organomet. Chem. 33 (2019) e4751. c) D. Gopalakrishnan, S. Srinath, B. Baskar, N.S.P. Bhuvanesh, M. Ganeshpandian, Appl. Organomet. Chem. 33 (2019) e4756. d) W. Ma, L. Guo, Z. Tian, S. Zhang, X. He, J. Li, Y. Yang, Z. Liu, Dalton Trans. 48 (2019) 4788-4793.

[21] G.M. Sheldrick, Crystal structure refinement with SHELXL, Acta Cryst. C. 71 (2015) 3-8.

[22] O.V. Dolomanov, L.J. Bourhis, R.J. Gildea, J.A.K. Howard, H. Puschmann, J. Appl. Crystallogr. 42 (2009) 339-341.

[23] H. Nawaz, Z. Akhter, S. Yameen, H.M. Siddiqi, B. Mirza, A. Rifat, J. Organomet. Chem. 694 (2009) 2198-2203.

[24] P.N. Kelly, A. Prêtre, S. Devoy, I. O'Rielly, R. Devery, A. Goel, J.F. Gallagher, A.J. Lough, P.T.M. Kenny, J. Organomet. Chem. 692 (2007) 1327-1331.

[25] B. Therrien, L. Vieille-Petit, J. Jeanneret-Gris, P. Štěpnička, G. Süss-Fink, J. Organomet. Chem. 689 (2004) 2456-2463.

[26] a) T.A. Peganova, I.S. Sinopalnikova, A.S. Peregudov, I.V. Fedyanin, A. Demonceau, N.A. Ustynyuk, A.M. Kalsin, Dalton Trans. 45 (2016) 17030-17041. b) Y.-W. Tsai, Y.-F. Chen, Y.-J. Li, K.-H. Chen, C.-H. Lin, J.-H. Huang, Molecules (Basel, Switzerland), 2018.

[27] Y.L.K. Tan, P. Pigeon, E.A. Hillard, S. Top, M.-A. Plamont, A. Vessières, M.J. McGlinchey, H. Müller-Bunz, G. Jaouen, Dalton Trans. (2009) 10871-10881.

[28] D. Pooja, H. Kulhari, L. Tunki, S. Chinde, M. Kuncha, P. Grover, S.S. Rachamalla, R. Sistla, RSC Adv. 5 (2015) 49122-49131.

[29] C. Praveen Kumar, T.S. Reddy, P.S. Mainkar, V. Bansal, R. Shukla, S. Chandrasekhar, H.M. Hügel, Eur. J. Med. Chem. 108 (2016) 674-686.

[30] E. Gottlieb, S.M. Armour, M.H. Harris, C.B. Thompson, Cell. Death Differ. 10 (2003) 709-717.

[31] N.P. Kumar, P. Sharma, T.S. Reddy, S. Nekkanti, N. Shankaraiah, G. Lalita, S. Sujanakumari, S.K. Bhargava, V.G.M. Naidu, A. Kamal, Eur. J. Med. Chem. 127 (2017) 305-317.

[32] J.M. Suski, M. Lebiedzinska, M. Bonora, P. Pinton, J. Duszynski, M.R. Wieckowski, Methods Mol Biol. 810 (2012) 183-205.

[33] A.V. Subba Rao, M.V.P.S. Vishnu Vardhan, N.V. Subba Reddy, T. Srinivasa Reddy, S.P. Shaik, C. Bagul, A. Kamal, Bioorg. Chem. 69 (2016) 7-19.

Journal Pre-proofs

Mixed metal ruthenium-ferrocene complexes with anti-cancer properties

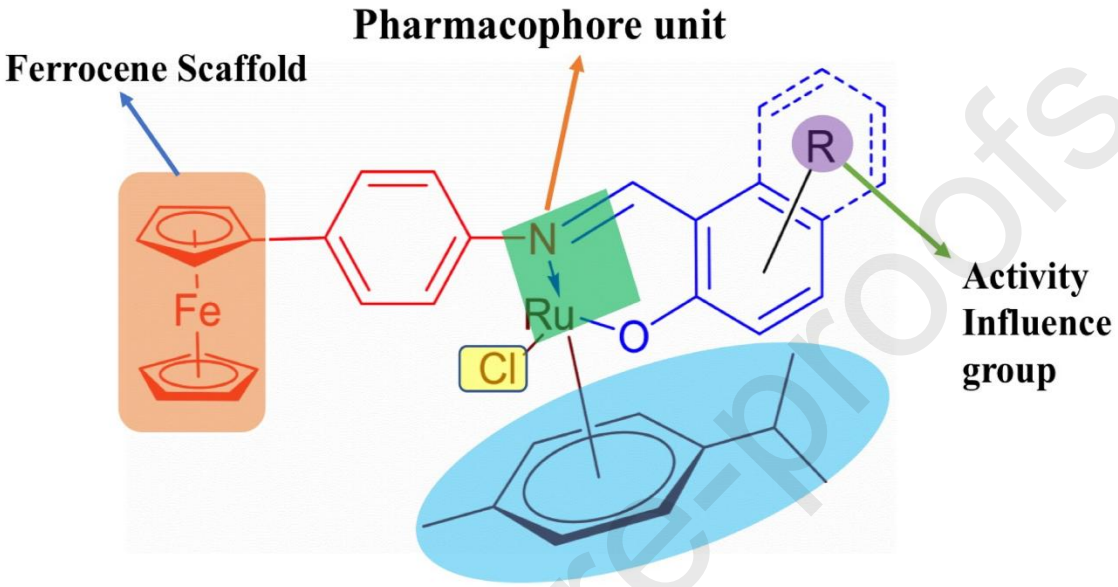

Journal Pre-proofs

Highlights

Six novel and fully characterized heterobimetallic Ru-Fe complexes are reported and their *in vitro* activities towards liver (HepG2) and human cervical (HeLa) cancer cell lines are reported.

Among the prepared complexes, **5c** and **5d** showed enhanced cytotoxicity towards HeLa and HepG2, with IC_{50} values of 9.34 and 15.74, respectively, compared to cisplatin (31.32 and 27.95, respectively).

Complex **5d** induced cell cycle arrest in the S phase and apoptosis through collapse of mitochondrial membrane potential and ROS.

Journal Pre-proofs

Journal Pre-proofs

CRediT authorship contribution statement

Ranjith kumar Jakku: Conceptualization, Methodology, Validation, Formal analysis, Investigation, Writing - original draft, Data curation. **Eda Rami Reddy:** Validation, Formal analysis. **Nedaossadat Mirzadeh:** Conceptualization, Methodology, Writing - review & editing, Supervision. **T. Srinivasa Reddy:** Data curation, software, investigation. **Anil Kumar Vardhaman:** Data curation, Software. **L. Giribabu:** Formal analysis, Validation. **Balasubramanian Sridhar:** Resources, formal analysis. **Deep Pooja:** Validation, Data curation. **Sistla Ramakrisna:** Resources, investigation. **Suresh Bhargava:** Supervision, Project administration, Funding acquisition. **Rajiv Trivedi:** Supervision, Formal analysis, Methodology.

Journal Pre-proofs